Argonne NATIONAL LABORATORY

ANL/ESD-21/6

Life Cycle Inventories for Palladium on Niobium Phosphate ($Pd/NbOPO_4$) and Zirconium Oxide (ZrO_2) Catalysts

Energy Systems Division

ANL/ESD-21/6

Life Cycle Inventories for Palladium on Niobium Phosphate ($Pd/NbOPO_4$) and Zirconium Oxide (ZrO_2) Catalysts

by
Kathryn Kingsbury and P. Thathiana Benavides
Energy Systems Division, Argonne National Laboratory

April 2021

CONTENTS

FIGURES

TABLES

ACKNOWLEDGEMENTS

The Bioenergy Technologies Office of the Office of Energy Efficiency and Renewable Energy of the United States supported this work (Contract DE-AC02-06CH11357). Kathryn Kingsbury's efforts were supported by the U.S. Department of Energy Science Undergraduate Laboratory Internship (SULI) Program during her internship in fall 2020 and spring 2021 at Argonne National Laboratory's Energy Systems Division. The authors would like to thank Uisung Lee of Argonne National Laboratory for generously sharing his time and effort working to implement new pathways into GREET, Ulises Gracida at Argonne for his support and instruction in using the GREET model, Donald Cronauer at Argonne for his guidance in examining the industrial scale-up of laboratory catalyst synthesis procedures, and Jarod Kelly, Amgad Elgowainy, and Troy Hawkins at Argonne for their constructive comments and helpful insights. The authors would also like to thank Glenn Hafenstine, Matthew Wiatrowski, and Derek Vardon of the National Renewable Energy Laboratory for providing information about the synthesis of the $Pd/NbOPO_4$ catalyst.

ABBREVIATIONS AND ACRONYMS

4-BH	4-butoxyheptane
Al_2O_3	aluminum oxide
$Al_2(SO_4)_3$	aluminum sulfate
Btu	British thermal units
CBMM	Companhia Brasileira de Metalurgia e Mineração
CO_2e	carbon dioxide equivalents
Co-Optima	DOE Co-Optimization of Fuels & Engines initiative
CSTR	Continuous-stir tank reactor
g	gram
gal	gallon
GHG	greenhouse gas
GREET	Greenhouse gases, Regulated Emissions, and Energy use in Technology
GWP	global warming potential
H_2	hydrogen gas
HMC	heavy-mineral concentrate
HNO_3	nitric acid
H_3PO_4	phosphoric acid
H_2SO_4	sulfuric acid
IWI	incipient wetness impregnation
K	Kelvin unit of temperature
kg	kilogram
kW	kilowatt
$KNbO_3$	potassium niobate
KOH	potassium hydroxide
L	liter
LCA	life cycle analysis
LCI	life cycle inventory
M	molarity
MJ	megajoule
MSP	mineral separation plant
mmBtu	million British thermal units

N_2	nitrogen gas
Na_2SiO_3	sodium silicate
Na_2ZrO_3	sodium zirconate
Nb	niobium
Nb_2O_5	niobium oxide or niobium pentaoxide
$NbOPO_4$	niobium phosphate
NREL	National Renewable Energy Laboratory
Pd	palladium
$Pd/NbOPO_4$	palladium on niobium phosphate catalyst
PGM	platinum group metal
Pt	platinum
t	metric tonne
TEA	technoeconomic analysis
ton	U.S. short ton
ZIA	Zircon Industry Association
ZrO_2	zirconium oxide or zirconia
$ZrSiO_4$	zircon, zircon sand, or zirconium silicate

EXECUTIVE SUMMARY

Purpose

Catalysts are used in refining and chemical processes to maximize product yield and reaction selectivity, and they are critically important in optimizing biofuel production to make biofuels a viable alternative to traditional fossil-based fuels. However, catalysts are rarely included in life cycle analysis (LCA) studies of biofuels due to lack of information. The catalyst module in Argonne National Laboratory's Greenhouse gases, Regulated Emissions, and Energy use in Technologies (GREET) model addresses this issue with catalyst energy and material data for use in biofuels LCAs (GREET 2020, Wang et al. 2015). Nevertheless, many catalysts remain to be analyzed, especially as new biofuel production pathways emerge, and catalyst technology advances. We therefore proposed to expand the GREET catalyst module with the addition of new catalyst materials applicable to current biofuel production pathways.

Approach

Before beginning this study, we performed an extensive literature review to assess current catalyst technology for biofuel production, and we selected two catalysts for incorporation into GREET: 1) palladium on a niobium phosphate support ($Pd/NbOPO_4$), and 2) zirconium oxide (ZrO_2). We then framed our analysis by tracing a cradle-to-gate supply chain for each catalyst. The supply chain for the $Pd/NbOPO_4$ catalyst required assessment of four precursor materials that were not available in GREET: niobium phosphate ($NbOPO_4$), potassium niobate ($KNbO_3$), niobium oxide (Nb_2O_5), and palladium (Pd). The supply chain for the ZrO_2 catalyst required assessment of only one precursor material not already in GREET: zircon ($ZrSiO_4$). We collected life cycle inventory (LCI) data for the two catalysts and five associated materials using publicly-available information, and we applied engineering calculations to estimate energy inputs for processes that lacked industrial data. Finally, we used the GREET model to calculate cradle-to-gate greenhouse gas (GHG) emissions, fossil fuel consumption, and water consumption for the $Pd/NbOPO_4$ and ZrO_2 catalysts and their associated materials.

Outcomes

We report the cradle-to-gate GHG emissions, fossil fuel consumption, and water consumption for Nb_2O_5, $KNbO_3$, $NbOPO_4$, Pd, $Pd/NbOPO_4$, $ZrSiO_4$, and ZrO_2. Notably, the net GHG emissions impact of the $Pd/NbOPO_4$ catalyst is 8.5 kg CO_2e/kg catalyst, which is comparable to other catalysts in GREET, while the net GHG emissions of the ZrO_2 catalyst is considerably lower at 1.8 kg CO_2e/kg catalyst. We also identify the primary contributors to each catalyst's cradle-to-gate environmental burden. For the $Pd/NbOPO_4$ catalyst, Pd metal is the main driver of GHG emissions and fossil fuel consumption, while Pd and $NbOPO_4$ contribute almost equally to water consumption. For the ZrO_2 catalyst, sodium hydroxide (NaOH) is the principal driver of GHG emissions and fossil fuel consumption, while $ZrSiO_4$ is the main consumer of water. The $Pd/NbOPO_4$ and ZrO_2 catalysts, as well as Nb_2O_5, $KNbO_3$, $NbOPO_4$, and $ZrSiO_4$, are implemented in the GREET catalyst module, and Pd has been implemented in GREET2 (Kingsbury and Benavides 2021). The material and energy flows for these new materials will be useful to future LCAs, particularly those involving biofuel production.

1. INTRODUCTION

Catalysts are employed across all sectors of the chemical industry to control selectivity and improve product yield in chemical processes. They are especially vital to the production of biofuels, which face many technical and economic obstacles to their industrial viability (Gaspar et al. 2019). A biofuel's eligibility for widespread adoption depends on several factors, including whether its life cycle greenhouse gas (GHG) emissions meet the guidelines of policies such as the U.S. Renewable Fuel Standard (RFS) and the California Low Carbon Fuel Standard (LCFS) (Benavides et al. 2017). Life cycle analysis (LCA) is used to determine these life cycle GHG emissions and other sustainability information about a biofuel. LCA is a valuable method for evaluating a product's environmental impact because it examines all stages in the product's supply chain, from extraction and processing of all raw materials to use and disposal of the final product. However, when LCA of a biofuel is performed, the contribution of the catalysts used in its production is frequently not accounted for due to lack of data and their minimal mass compared with other process inputs. As the impacts of catalysts may be more significant than would be indicated by their small mass input to the process, it is relevant to provide inventories for the catalysts associated with new biofuel production pathways.

In this study, we specifically examine two catalysts that are relevant to biofuel production. The first is a single-phase catalyst composed of palladium metal on a niobium phosphate support ($Pd/NbOPO_4$) developed by Hafenstine et al. (2020), and the second is a traditional zirconium oxide (ZrO_2) catalyst. We have selected these catalysts for a variety of reasons. Both catalysts may be applied in the conversion of biomass to 4-butoxyheptane (4-BH), an ether diesel bioblendstock that is currently of interest to the U.S. Department of Energy's (DOE's) Co-Optimization of Fuels & Engines (Co-Optima) initiative due to its outstanding fuel properties and potential for industrial viability (Huq et al. 2019). The production of 4-BH from biomass requires multiple chemical reactions and thus multiple catalysts: ZrO_2 serves as a ketonization catalyst and $Pd/NbOPO_4$ as a reductive etherification catalyst. The $Pd/NbOPO_4$ catalyst is especially noteworthy because the Pd active phase assists in hydrogenation chemistry, while the $NbOPO_4$ support acts as a solid acid catalyst for ketalization and dehydration chemistry (Hafenstine et al. 2020). Both the ZrO_2 and $Pd/NbOPO_4$ catalysts have displayed high conversion rates for their respective reactions during 4-BH production (Hafenstine et al. 2020).

Both ZrO_2 and $Pd/NbOPO_4$ also show promise as effective catalysts for producing biofuels other than 4-BH. For the synthesis of biodiesel, ZrO_2 has been successfully used as a catalyst in a sulfated form, in an acid-modified form, and as a support for tungstates (ZIA 2019). There are also ongoing efforts to use ZrO_2-supported metal catalysts in the reforming of gasoline, diesel, butane, propane, and ethanol (ZIA 2019). Most notably, ZrO_2 has already been employed in a study by the National Renewable Energy Laboratory (NREL) as a ketonization catalyst during production of a diesel and jet fuel range blendstock (Davis et al. 2018). The $Pd/NbOPO_4$ catalyst is also very likely to be applicable in additional biofuel production pathways due to the valuable catalytic properties of Pd and Nb compounds. Palladium is a

member of the platinum group metals (PGMs), which are widely used in catalysis due to their unique chemical properties and high degree of stability (Kettler 2003). Palladium and other PGM catalysts are especially relevant to the biofuel industry because they can assist reactions such as hydrogenations and oxidations that are common in many different biofuel production pathways. Niobium compounds are also of great interest in the field of catalysis due to their ability to function in different scenarios as catalyst active phases, catalyst supports, solid acid catalysts, or redox materials (Nowak and Ziolek 1999). Niobic acid, which is analogous to hydrated Nb_2O_5, has been used as a ketone condensation catalyst in the same pathway as ZrO_2 to produce diesel and jet fuel range blendstock (Davis et al. 2018). Niobium phosphate is also especially useful due to its strong surface acidity even at the high temperatures used in pretreatment processes (Nowak and Ziolek 1999). Many opportunities therefore exist for application of our chosen catalysts in future LCA studies.

In this work, we examine the consumption of material and energy inputs throughout the life cycle of the $Pd/NbOPO_4$ and ZrO_2 catalysts. The scope of our analysis for both catalysts is cradle-to-gate, which refers to all stages in catalyst production from the extraction and processing of raw materials up to the manufacturing facility gate. In Section 2.1, we define a supply chain for $Pd/NbOPO_4$ and describe the collection of life cycle inventory (LCI) data from various sources detailing the individual stages in the $Pd/NbOPO_4$ catalyst supply chain. We specifically examine five primary stages: 1) production of Nb_2O_5 from the mining of pyrochlore, 2) chemical synthesis of $KNbO_3$ from Nb_2O_5, 3) chemical synthesis of $NbOPO_4$ from $KNbO_3$, 4) production of Pd metal from the mining and processing of PGMs, and 5) synthesis of the $Pd/NbOPO_4$ catalyst by incipient wetness impregnation (IWI) of the Pd metal onto the $NbOPO_4$ support. In Section 2.2, we define the supply chain and LCI collection for the ZrO_2 catalyst and examine two primary production stages: 1) production of zircon from the mining and beneficiation of heavy-mineral sands, and 2) ZrO_2 catalyst production by caustic fusion and calcination of zircon. If co-products are produced alongside the catalyst, we apply a mass allocation approach that allocates material and energy consumption to the major product, thus remaining consistent with existing materials in the GREET catalyst module (GREET 2020). In Section 3, we use the GREET model to calculate cradle-to-gate values for GHG emissions, fossil fuel consumption, and water consumption for all new materials. GHG emissions are reported in units of kg CO_2e, fossil fuel consumption in units of MJ, and water consumption in units of gal. All three metrics are reported per kg of catalyst or associated material produced. While we do not report or discuss LCA results for the generation of criteria air pollutants (CAPs) in this work, these values are available in GREET for the new catalysts and associated materials (GREET 2020). Finally, we provide a discussion of the factors that contribute to the net environmental impact of the $Pd/NbOPO_4$ and ZrO_2 catalysts that will be beneficial to the design and selection of new catalyst materials. Both catalysts and their associated materials are implemented in the GREET model for use in future LCA studies.

2. DATA AND METHODOLOGY

2.1 LIFE CYCLE INVENTORY OF $Pd/NbOPO_4$ CATALYST

A product's LCI identifies and quantifies all resources and energy used throughout the product's life cycle. Using the LCI, an LCA can then assess the product's total environmental impact. Before compiling LCI data for the $Pd/NbOPO_4$ catalyst, it is necessary to identify a supply chain for the catalyst that traces each contributing material back to the beginning of its own life cycle. Many different pathways may be followed to eventually produce the $Pd/NbOPO_4$ catalyst, but data on industrial catalyst production is very limited. The $Pd/NbOPO_4$ supply chain that we show in Figure 1 is thus based on a combination of processes for which material and energy inputs are either publicly available or can be calculated using chemical and engineering principles. As depicted in Figure 1**,** niobium oxide (Nb_2O_5) is produced from the mining and processing of pyrochlore ore. Niobium oxide is then converted to an intermediate chemical, potassium niobate ($KNbO_3$), which is subsequently converted to the niobium phosphate ($NbOPO_4$) catalyst support. Palladium (Pd) metal, which is produced from the mining and processing of the platinum group metals (PGMs), is then added to the niobium phosphate support, and several processing steps are performed to produce the final $Pd/NbOPO_4$ catalyst. In the following subsections, we describe each of these production stages in greater detail.

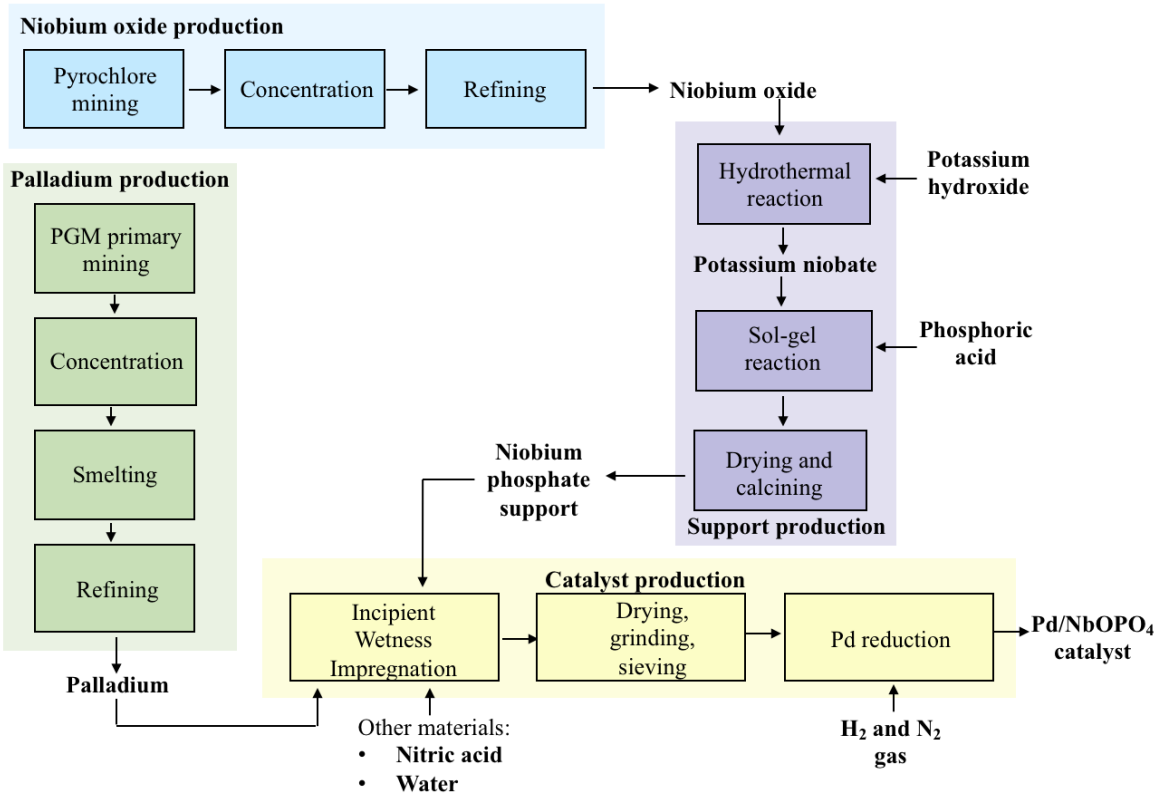

Figure 1. Supply chain featuring the primary material inputs and outputs for production of the $Pd/NbOPO_4$ catalyst

To obtain LCI data for the $Pd/NbOPO_4$ catalyst, we consulted a variety of sources, including scientific literature, technical reports from Argonne and other national laboratories, sustainability reports from mining and chemical companies, information already in the GREET model, and direct correspondence with experts in the field. The final step in the production of the $Pd/NbOPO_4$ catalyst, IWI, is described by Hafenstine et al. (2020). This process requires Pd metal, $NbOPO_4$, nitric acid (HNO_3), hydrogen (H_2) gas, and nitrogen (N_2) gas. Data on the last three materials can be found in the GREET model (GREET 2020). The production of Pd as a PGM and its implementation in GREET is described by Kingsbury and Benavides (2021). The $NbOPO_4$ support can be produced from the reaction of potassium niobate ($KNbO_3$) and phosphoric acid (H_3PO_4) using a sol–gel method detailed by both Wang et al. (2018) and He et al. (2020). Life-cycle data for H_3PO_4 is already available in the GREET model (GREET 2020), and we traced $KNbO_3$ through its synthesis from the hydrothermal reaction of Nb_2O_5 with potassium hydroxide (KOH) as described by Lu et al. (1998). Life-cycle data for KOH is found in the GREET model (GREET 2020), and we describe the production of Nb_2O_5 from pyrochlore as reported by Companhia Brasileira de Metalurgia e Mineração (CBMM 2019). Note that for the IWI synthesis of the $Pd/NbOPO_4$ catalyst, the sol–gel synthesis of $NbOPO_4$, and the hydrothermal synthesis of $KNbO_3$, only laboratory-scale material inputs and processing steps were available. We therefore use stoichiometric ratios to estimate material requirements on an industrial scale, and we utilize an estimation technique devised by Majeau-Bettez et al. (2011) and presented in Dunn et al. (2015) to calculate the energy consumption required for these processes.

2.1.1 Niobium oxide production from pyrochlore mining and processing

Niobium is not found in nature as a free element and is most commonly sourced from the mineral pyrochlore, which is found within alkaline igneous rock deposits (Schulz et al. 2017). Brazil contains the world's largest deposits of pyrochlore and serves as the global leader in niobium production, responsible for 88% of all niobium production worldwide (Padilla 2020). Based in Araxà, Brazil, CBMM owns the largest share of pyrochlore mines and produces more niobium products each year than any other company, so for the purposes of our study we focused on the production methods and data from this company's official sustainability reports (CBMM 2019). These pyrochlore deposits contain an average of 2.5% Nb_2O_5 content, so several processes are required to concentrate the Nb_2O_5 and separate it from the other materials also obtained from pyrochlore (CBMM 2019).

Pyrochlore ore is mined using open-pit methods and transported by electric-powered conveyor belts to the blending yard and concentration plant where the non-niobium-containing components of the pyrochlore are removed by grinding, magnetic separation, desliming, and flotation. Pyrometallurgy processing of the niobium concentrate removes contaminants such as phosphorous, sulfur, and lead. Depending on the desired end product, the niobium concentrate is further processed in a variety of ways. Although approximately 90% of the niobium that is extracted from pyrochlore is processed and sold as ferroniobium, an iron-niobium alloy used in steel materials, CBMM also produces a significant amount of laboratory-grade niobium

chemicals like Nb_2O_5. In this case, the niobium concentrate is taken to a high-purity niobium oxide plant and a specialized oxides plant where it is purified to 99.5% Nb_2O_5 (CBMM 2019). CBMM conducts all mining, concentrating, and production processes on-site and exports only finished niobium products.

CBMM sustainability reports for 2016, 2017, 2018, and 2019 include the total niobium production, material inputs, and energy consumption per year. The average yearly production of total niobium products during this time period was 862,750 tons. Approximately 89% of this total consisted of ferroniobium products, with the remaining 11% of production being composed of other niobium products such as Nb_2O_5. CBMM details the amount of petroleum coke, charcoal, water, electricity, diesel fuel, and liquefied petroleum gas that is consumed during the overall production process each year. This data represents all of the materials and energy that went into producing all niobium products, beginning with the mining of pyrochlore ore and ending at the point of commercial distribution of the final niobium products. CBMM also reports minimal consumption of aviation fuel and biodiesel, but we omitted these from our inventory because their combined contribution to the total energy input was less than 0.1% and because detailed information regarding their exact application in Nb_2O_5 production was not provided. Using a mass allocation approach, we determined the material and energy inputs per ton of Nb_2O_5 product (Table 1)**.** Upstream information regarding petroleum coke, diesel fuel, liquefied petroleum gas, and electricity generation in Brazil is available in GREET (GREET 2020). To determine upstream information for charcoal, we use the same approach presented in Benavides et al. (2015) and model charcoal production from the pyrolysis of willow, the energy and emissions burdens of which are detailed in GREET (GREET 2020).

Table 1. Material and energy inputs for the production of Nb_2O_5

Material	**Amount per ton Nb_2O_5**	
Petroleum coke	0.0037 tons	
Charcoal	0.0135 tons	
Water	542 gal	
Energy	**mmBtu/ton Nb_2O_5**	**Share %**
Electricity	1.212	72%
Diesel	0.149	9%
Liquefied petroleum gas	0.320	19%
Total energy input	1.681	

2.1.2 Preparation of potassium niobate precursor by hydrothermal synthesis

Potassium niobate ($KNbO_3$) can be synthesized from Nb_2O_5 and KOH using a variety of methods such as hydrothermal, solid-state, and precipitation reactions. We chose to explore the hydrothermal method because it requires significantly lower reaction temperatures compared to the other two methods (Lu et al. 1998), and it is associated with high product yield and quick reaction time (Rashid et al. 2018). Hydrothermal synthesis occurs within a sealed vessel, usually an autoclave, where extremely high pressures enable a solvent to be heated past its normal boiling point without evaporating. The high temperature and pressure promote the rapid interaction and assembly of the particles dissolved in the solvent (Rashid et al. 2018).

We examined a procedure for the laboratory-scale hydrothermal synthesis of $KNbO_3$ described by Lu et al. (1998). In this procedure, solid KOH is dissolved in water to prepare an 8 M KOH solution, which is then mixed with 3.32 g of Nb_2O_5. The total volume of solution is set to 125 mL, so the Nb_2O_5 has a concentration of 0.1 M. The solution is placed into a sealed autoclave reactor and heated at 200°C for 2 hours while being continuously stirred. After hydrothermal reaction (see Equation 1) the $KNbO_3$ product obtained is washed and dried.

$$Nb_2O_5 + 2\,KOH \rightarrow 2\,KNbO_3 + H_2O \quad (1)$$

To estimate the quantities of materials used, we assumed a 100% yield of the $KNbO_3$ product and used the reaction's stoichiometric ratios to relate the mass inputs of Nb_2O_5, the limiting reagent, to the mass of $KNbO_3$ produced. Since excess KOH is used, we assumed that all KOH that is not consumed during the reaction is recycled and may be re-used as a reactant. Finally, we assumed that the H_2O formed during reaction can be recycled for use as a solvent, and we used a conservative estimate that 50% of the water used as a solvent may be recycled by purification.

To estimate energy consumption for the production of $KNbO_3$, we adopted the methodology of Majeau-Bettez et al. (2011) and Dunn et al. (2015). In this method, the total energy of production is equivalent to the sum of the energy needed to heat any materials plus the energy required to power any equipment used. On an industrial scale, the hydrothermal reaction may be performed in a continuous-stir tank reactor (CSTR). The total energy ($q_{t,KNbO_3}$) required to produce 1 ton of $KNbO_3$ is calculated as the sum of the heat required to heat the reaction solvent ($q_{solvent}$), the heat loss of the reactor (q_{CSTR}), and the energy used in stirring the materials (q_{stir}). The energy required to dry the product is assumed to be negligible in this scenario as the product does not require intensive heat-treating. A key assumption in the total energy calculation is that half of the heat used to heat the solvent may be recovered and re-incorporated by heat integration, causing the value of $q_{solvent}$ to be halved (Equation 2).

$$q_{t,KNbO_3} = \frac{q_{solvent}}{2} + q_{CSTR} + q_{stir} \quad (2)$$

A detailed account of the calculations for each term in Equation 2 can be found in Appendix A. The volume of the reactor is assumed to be 10,000 L, which we used to scale the energy consumption according to the amount of material required to produce 1 ton of $KNbO_3$. Heating of the reactor and solvent consumes natural gas that is combusted in a boiler with a 90% efficiency, while the energy used for stirring is electricity. Table 2 summarizes the total material and energy inputs for the production of $KNbO_3$ from the hydrothermal reaction of Nb_2O_5 and KOH.

Table 2. Material and energy inputs for the production of $KNbO_3$

Material	**Amount per ton $KNbO_3$**	
Nb_2O_5	0.738 tons	
KOH	0.312 tons	
Water	3,325 gal	
Energy	**mmBtu/ton $KNbO_3$**	**Share %**
Electricity	0.100	1%
Natural gas	7.886	98%
Total energy input	7.986	

Because the hydrothermal method requires continuous maintenance of high pressures and involves the heating of solvents with high specific heat capacities, it is quite energy intensive in terms of natural gas and water consumption.

2.1.3 Production of niobium phosphate support by sol–gel synthesis

Niobium phosphate ($NbOPO_4$) is commonly produced by the reaction of potassium niobate ($KNbO_3$) with phosphoric acid (H_3PO_4). This approach is used by Wang et al. (2018) and He et al. (2020), who both describe a sol–gel method for this reaction. This method involves the stimulation of small molecules to form a colloidal solution, which then evolves to form a gel with a liquid and a solid phase. The liquid phase is then removed by drying the solvent (Rashid et al. 2018).

We analyzed a laboratory-scale sol–gel synthesis of $NbOPO_4$ that draws from the procedures of both Wang et al. (2018) and He et al. (2020). In this process, 1.15 g of 85% H_3PO_4 is dissolved in 25 mL of water, and a 0.1 M $KNbO_3$ solution is added to the H_3PO_4 solution. Using the stoichiometric ratios of the reaction (see Equation 3), we determined that 1.80 g of pure $KNbO_3$ is reacted with the H_3PO_4 and that the total volume of solution is 124.75 mL, giving a concentration of 0.4 M for H_3PO_4. The solution is stirred for 1 hour at 40°C and for 2 additional hours at 80°C. It is then heated in a sealed autoclave reactor at 160°C for 24 hours. After cooling, the product is filtered, washed, and dried at 110°C overnight or for approximately 12 hours. Finally, the solid product is calcined at 400°C for 3 hours to obtain a catalyst-quality $NbOPO_4$ product.

$$KNbO_3 + H_3PO_4 \rightarrow NbOPO_4 + KOH + H_2O \quad (3)$$

In order to estimate the quantities of material in industrial production, we assumed a 100% yield of the $NbOPO_4$ product and used the reaction's stoichiometric ratios to relate the mass inputs of $KNbO_3$ and H_3PO_4 to the mass of $NbOPO_4$ produced. We considered KOH to be a coproduct of $NbOPO_4$, and we used a mass allocation approach to calculate the environmental burden of this synthesis based on 79% of the products consisting of $NbOPO_4$ and 21% consisting of KOH. We again assumed that the H_2O formed during reaction can be recycled for use as a solvent, and we used a conservative estimate that 50% of the total water that is used as a solvent may be recycled after purification.

To estimate energy consumption for the production of $NbOPO_4$, we adopted the methodology of Majeau-Bettez et al. (2011) and Dunn et al. (2015) as we did with the production of $KNbO_3$, but we expanded the total energy consumption to include drying and calcining, as these are important steps in achieving a catalyst-grade product. On an industrial scale, reaction and solvent heating within the autoclave may be modeled using a CSTR, while drying occurs in a chamber oven and calcining in a chamber furnace. The total energy ($q_{t,NbOPO_4}$) required to produce 1 ton of $NbOPO_4$ is calculated as the sum of the heat required to heat the reaction solvent ($q_{solvent}$), the heat loss by the reactor (q_{CSTR}), the heat required to dry the $NbOPO_4$ product (q_{dry}), the energy used in heating the oven (q_{oven}), the heat required to calcine the $NbOPO_4$ product ($q_{calcine}$), the energy used in heating the furnace ($q_{furnace}$), and any energy used in stirring the materials (q_{stir}). We assume that half of the heat consumed during the heating of any materials, either in solution or as dry $NbOPO_4$, may be recovered and re-incorporated into the process by heat integration, causing the values of $q_{solvent}$, q_{dry}, and $q_{calcine}$ to be halved (Equation 4).

$$q_{t,NbOPO_4} = \frac{q_{solvent}}{2} + q_{CSTR} + \frac{q_{dry}}{2} + q_{oven} + \frac{q_{calcine}}{2} + q_{furnace} + q_{stir} \quad (4)$$

More details regarding the calculations for each term in Equation 4 can be found in Appendix B. As with the production of $KNbO_3$, we scaled the energy consumption to 1 ton of $NbOPO_4$ by relating the interior volume of any equipment used to the amount of material that must be loaded into the equipment in order to produce 1 ton of $NbOPO_4$. The same steam-powered CSTR with a volume of 10,000 L that is described by Majeau-Bettez et al. (2011) may be used to heat the solvent in the first step. We modeled the drying step using a 1,000 L chamber oven and the calcining step using an 8,300 L chamber furnace. Both the chamber oven and chamber furnace are from Nabertherm and are powered by electricity (Nabertherm 2016).

Table 3 summarizes the total material and energy inputs for the production of $NbOPO_4$ from the sol–gel reaction of $KNbO_3$ and H_3PO_4.

Table 3. Material and energy inputs for the production of $NbOPO_4$

Material	**Amount per ton $NbOPO_4$**	
$KNbO_3$	0.692 tons	
H_3PO_4	0.377 tons	
Water	5,756 gal	
Energy	**mmBtu/ton $NbOPO_4$**	**Share %**
Electricity	0.446	3%
Natural gas	13.341	97%
Total energy input	13.788	

The production of $NbOPO_4$ is quite intensive in terms of natural gas and water consumption. A large amount of water is required to obtain the correct concentration of reactants during the sol–gel synthesis procedure. The need to heat all of this water in the CSTR leads to heavy consumption of the natural gas used to power the CSTR.

2.1.4 Palladium metal production from PGM mining and processing

Palladium metal is produced in conjunction with the other platinum group metals (PGMs): platinum, palladium, rhodium, ruthenium, iridium, and osmium. PGMs are found as mixed metal and mineral deposits along with gold, nickel and copper within basic igneous rocks (Seymour and O'Farrelly 2012). The Bushveld Igneous Complex in South Africa contains the largest PGM deposits in the world and produces over 70% of the world's supply of PGMs. These deposits contain 5-8 g of PGM content per metric tonne (t) of ore, and 20% to 25% of this PGM content is palladium (Seymour and O'Farrelly 2012). This gives a maximum palladium content of only 0.0002% in the ore, so intensive processing is required to procure palladium from these mixed ore deposits. The typical process stages for PGM production are mining, concentrating, smelting, and refining (Benavides et al. 2015).

Conventional underground or open cut techniques are used for mining the PGM ore, which is located at depths between 500 m and 2 km in South African deposits, requiring large energy inputs for drilling, ore hauling, and refrigeration (Benavides et al. 2015). The mined ore is then crushed and milled into small particles and mixed with water to form a slurry for concentration, where froth flotation is employed to separate waste from the valuable minerals, producing a concentrate with a 100-150 g/t PGM content (Seymour and O'Farrelly 2012). Gravity separation may be used at this point to further separate larger PGM particles, while the majority of the concentrate is smelted in electric furnaces and slow-cooled to produce a matte with a 1500 g/t PGM content as well as nickel, copper, and iron sulfides. (Seymour and O'Farrelly 2012). The iron and sulfur content are decreased with oxygen-enriched air, and

magnetic separation removes nickel and copper from the rest of the PGMs, producing a final concentrate with a 50%-60% PGM content. Finally, a variety of refining techniques such as solvent extraction, distillation, and ion-exchange further increase PGM content in the concentrate and separate the PGMs from each other. In the case of palladium, an aqua regia process is generally used to dissolve the PGM concentrate before treatment with ammonium hydroxide and hydrochloric acid to precipitate a solid palladium complex (Seymour and O'Farrelly 2012).

Kingsbury and Benavides (2021) provide water and energy inputs for the production of palladium by mining, concentrating, smelting, and refining the PGMs. This data, along with inputs for three other PGM production pathways, has already been incorporated into the GREET2 model (GREET 2020). The data reported by Kingsbury and Benavides (2021) is sourced from Anglo American Platinum, a South African mining company that operates seven mines in the Bushveld Complex. From 2015 to 2019, Anglo American Platinum reported its average annual energy and water consumption for the production of all their products: palladium, platinum, rhodium, gold, iridium, ruthenium, nickel, and copper. These reported values correspond to the total inputs across the mining, concentrating, smelting, and refining stages. Information about potential process chemicals or materials used in PGM refining and separation was not provided by Anglo American Platinum and thus is not included in this inventory, but we assume that their contribution to the total energy consumption is minimal. Kingsbury and Benavides (2021) determined the division of the total energy input by fuel type (electricity, diesel, coal, and natural gas). For consistency with other catalyst materials in the GREET model (GREET 2020), we used energy inputs for palladium that were calculated from the total production energy by mass allocation, which is set as the default method in GREET. Kingsbury and Benavides (2021) also discuss market allocation as an option for calculating the energy inputs per ton of Pd, so we provide these inputs and the corresponding LCA results in Appendix D. Palladium is a high-value metal, especially in comparison to nickel and copper which are also produced by Anglo American Platinum, so the energy consumption of Pd production is considerably higher when using market allocation as opposed to mass allocation. The inputs for the production of 1 ton of palladium using the results of the mass allocation approach (Kingsbury and Benavides 2021) are presented in Table 4**.**

Table 4. Material and energy inputs for the production of palladium

Material	**Amount per ton Pd**	
Water	171,176 gal	
Energy	**mmBtu/ton Pd**	**Share %**
Electricity	340.1	71%
Diesel	54.8	11%
Coal	80.1	17%
Natural gas	4.9	1%
Total energy input	479.1	

Palladium production is extremely resource-intensive due to the very low PGM content (≤0.0002%) in mined ore, which requires considerable energy and water inputs for extraction and beneficiation. For comparison, the Nb_2O_5 content in the pyrochlore ore from which it is extracted is approximately 2.5%, leading to significantly smaller energy and material requirements. We note that palladium and other PGMs may also be recovered by recycling, or secondary production, which would significantly reduce their environmental burden. Secondary production of palladium involves smelting or dissolving a palladium-containing product, and then refining this molten matte or solution to separate out the palladium in a purified form (Benavides et al. 2015). Palladium and other PGMs display an extremely high recovery rate at 98%-99% (Seymour and O'Farrelly 2012) after undergoing the processes of secondary production. Information about the material and energy inputs for the secondary production of palladium was not available, so we did not account for this pathway in our inventory, but it would be worthwhile to examine in future LCA studies.

2.1.5 Production of $Pd/NbOPO_4$ catalyst by incipient wetness impregnation

To produce the $Pd/NbOPO_4$ catalyst, Pd is deposited on the $NbOPO_4$ support using IWI. In this method, the active phase metal is first dissolved in an acid and then drawn into the pores of the catalyst support through capillary action. Calcination then eliminates any volatile compounds from the metal or support (Rashid et al. 2018).

We examined the procedure of Hafenstine et al. (2020) for the IWI synthesis of $Pd/NbOPO_4$. Pd metal is dissolved in a nitric acid (HNO_3) solution and mixed with $NbOPO_4$ for 12 hours. The catalyst slurry is dried under air at 107°C for 6 hours and at 265°C for 2 hours. The dried product is ground and sieved into mesh particles. The product is then purged under nitrogen (N_2) gas for 1 hour. Finally, Pd ions are reduced to Pd metal by heating the product to 265°C and reducing with hydrogen (H_2) gas for 5 hours, forming the $Pd/NbOPO_4$ catalyst.

Quantities of materials for industrial production of $Pd/NbOPO_4$ were provided by direct correspondence with manufacturers of the catalyst (G. Hafenstine, pers. comm.). We also consulted the parameters for $Pd/NbOPO_4$ production listed in the CatCost software, a tool that allows researchers to estimate the large-scale production costs of pre-commercial catalysts (CatCost 2019) and which Hafenstine et al. (2020) used to incorporate the $Pd/NbOPO_4$ catalyst into a technoeconomic analysis (TEA). We verified that the material inputs and process steps that we used to estimate energy inputs for catalyst production were reflective of the procedure in CatCost. Hafenstine et al. (2020) designed the catalyst synthesis so that the Pd active phase in the $Pd/NbOPO_4$ catalyst is 5% by weight. The amount of N_2 and H_2 gas required for purging is based on a flow rate of 200 mL/min for both gases. We again assumed that 50% of the water that is used as a solvent may be recycled after purification.

We again estimated the energy consumption for the production of $Pd/NbOPO_4$ by taking the sum of the energy consumed in heating any materials plus the energy required to power any equipment (Majeau-Bettez et al. 2011, Dunn et al. 2015). In this scenario, we modeled the

stirring of materials using an electrically powered industrial chemical mixer that is capable of agitating catalyst slurries. The catalyst is dried in two stages at different temperatures, both of which may be modeled using a chamber oven, while heating of the catalyst under H_2 gas requires a tube furnace. The total energy ($q_{t,Pd/NbOPO_4}$) required to produce 1 ton of the Pd/$NbOPO_4$ catalyst is calculated as the sum of the heat required to dry the catalyst in two stages at 107°C (q_{dry_1}) and 265°C (q_{dry_2}), the heat used in heating the oven to 107°C (q_{oven_1}) and to 265°C (q_{oven_2}), the heat required to reduce the Pd/$NbOPO_4$ catalyst under H_2 gas (q_{reduce}), the energy used in heating the tube furnace for this reduction (q_{tube}), and the energy used in stirring the materials (q_{stir}). We assumed that half of the heat consumed by the Pd/$NbOPO_4$ material in any stage may be recovered and re-incorporated, causing the values of q_{dry_1}, q_{dry_2}, and q_{reduce} to be halved (Equation 5).

$$q_{t,Pd/NbOPO_4} = \frac{q_{dry_1}}{2} + q_{oven_1} + \frac{q_{dry_2}}{2} + q_{oven_2} + \frac{q_{reduce}}{2} + q_{tube} + q_{stir} \qquad (5)$$

An explanation of each individual term in Equation 5 is provided in Appendix C. In order to scale the energy consumption to the production of 1 ton of Pd/$NbOPO_4$, we modeled both drying steps using a chamber oven with a volume of 1,050 L (Nabertherm 2016). While stirring was performed in the CSTR for the production of $KNbO_3$ and $NbOPO_4$, in this case the stirring is performed using a chemical mixer that can agitate catalyst slurries up to 1,892 L (Madden Pump 2020). The interior volume of the tube furnace used for reduction is calculated based on a provided tube radius of 50 mm and a heated length of 100 mm (Nabertherm 2017). Table 5 summarizes the total material and energy inputs for the production of Pd/$NbOPO_4$. Compared to the rest of the processing steps in the supply chain of the Pd/$NbOPO_4$ catalyst, the final synthesis of the catalyst by IWI is minimally energy intensive.

Table 5. Material and energy inputs for the production of Pd/$NbOPO_4$

Material	**Amount per ton Pd/$NbOPO_4$**
Pd	0.05 tons
HNO_3	0.05 tons
$NbOPO_4$	0.95 tons
N_2 gas	0.0058 tons
H_2 gas	0.0021 tons
Water	72 gal

Energy	**mmBtu/ton Pd/$NbOPO_4$**	**Share %**
Electricity	0.496	100%
Total energy input	0.496	

2.2 LIFE CYCLE INVENTORY OF ZrO_2 CATALYST

As with our analysis of the $Pd/NbOPO_4$ catalyst, it is first necessary to identify a cradle-to-gate supply chain for production of the ZrO_2 catalyst based on publicly available data. ZrO_2 is a commonly used material in many industrial processes, and it may adopt several different crystal structures and morphologies with differing properties and applications (ZIA 2019). For the purposes of this study, we specifically outlined a pathway for the production of a pure monoclinic ZrO_2 catalyst, as this is the form used in the production pathway of the 4-BH biofuel (G. Hafenstine, pers. comm.). Zirconium compounds such as ZrO_2 may be sourced from many different zirconium-containing minerals, such as baddeleyite and eudialyte, but we limited our focus to zircon ($ZrSiO_4$) since this is the most commonly used commercial zirconium mineral (Nielsen et al. 2012).

As depicted in Figure 2**,** zircon is produced by the mining, beneficiation, and separation of mineral sands. Zircon is then decomposed by caustic fusion with NaOH to yield sodium zirconate (Na_2ZrO_3) as well as a sodium silicate (Na_2SiO_3) byproduct. Na_2ZrO_3 then hydrolyzes to form hydrous zirconia which is calcined at the production plant to form commercial ZrO_2. Finally, the commercial ZrO_2 is further calcined at high temperatures to yield catalyst-grade ZrO_2 with a monoclinic crystal structure. We describe these production processes in further detail in the following subsections.

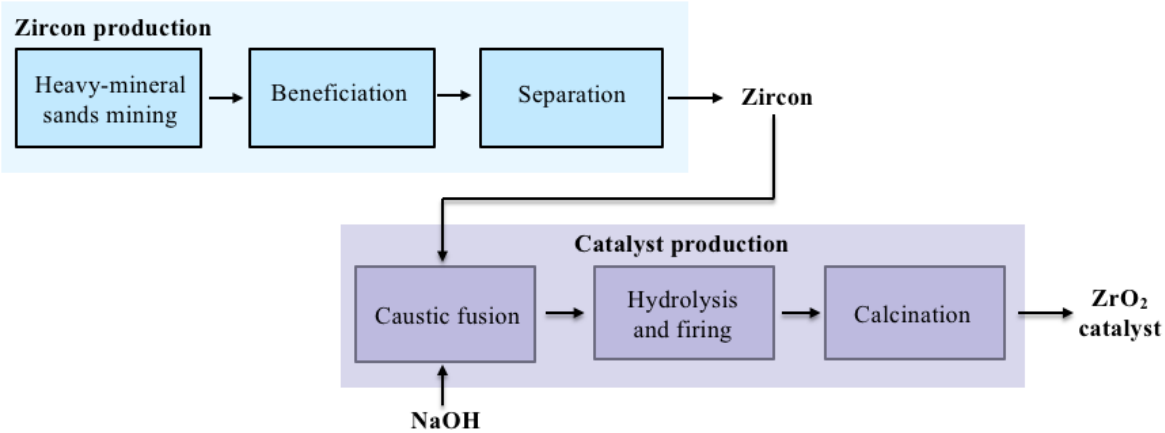

Figure 2. Supply chain featuring the primary material inputs and outputs for production of the ZrO_2 catalyst

We again consulted a variety of sources, from scientific literature to the GREET database, in order to determine the material and energy inputs for the LCI of the ZrO_2 catalyst. For the final calcination of commercial ZrO_2 to a monoclinic catalyst product, we examined a laboratory procedure from Shylesh et al. (2017), which requires no material inputs other than commercial ZrO_2. For the decomposition of $ZrSiO_4$ to Na_2ZrO_3, hydrolysis of Na_2ZrO_3 to hydrous zirconia, and calcination of hydrous zirconia to commercial ZrO_2, we used an inventory from Primas (2007). Other than the $ZrSiO_4$ material input, the process steps in this inventory required only one additional material input, NaOH, the life cycle data of which is available in

GREET (GREET 2020). All inputs for the production of zircon from the mining, beneficiation, and separation of mineral sands are described by Gediga et al. (2019). Additional material inputs of NaOH, sulfuric acid (H_2SO_4), aluminum sulfate ($Al_2(SO_4)_3$), and lubricating oil were required for the production of $ZrSiO_4$. Both NaOH and H_2SO_4 are detailed in GREET (GREET 2020). We used estimations to input $Al_2(SO_4)_3$ and lubricating oil, since these materials are not in GREET and contribute only very slightly to $ZrSiO_4$ production. $Al_2(SO_4)_3$ may be produced from the reaction of H_2SO_4 with aluminum oxide (Al_2O_3) (Darragh and Ertell 2003), both of which are available in the GREET model (GREET 2020), so we used stoichiometry to calculate the amount of Al_2O_3 and H_2SO_4 needed to produce the necessary amount of $Al_2(SO_4)_3$ for $ZrSiO_4$ production. We assumed no additional energy is required for this chemical reaction and included Al_2O_3 and H_2SO_4 as material inputs in place of $Al_2(SO_4)_3$. We used gasoline blendstock as a surrogate for lubricating oil, which is produced from the refining and distillation of crude oil much like gasoline (Sullivan 2005). When implementing vehicle fluids such as engine oil, which is analogous to lubricating oil, into GREET2, Burnham et al. (2006) estimated energy and emissions using gasoline manufacturing, so we adopted the same approach in our inventory.

2.2.1 Production of zircon by mining, beneficiation, and separation of mineral sands

Zircon forms naturally by crystallization as a mineral within silica-containing rocks such as granites, syenites, and diorites (ZIA 2019). The zircon contained in these primary ore deposits is largely inaccessible or minimally concentrated, so the majority (97%) of zircon is obtained from secondary placer deposits of heavy-mineral sands (ZIA 2019). These sand deposits have developed over millions of years as weathering and erosion have worn away at zircon-containing rocks, while wind and water have concentrated and transported the heavy zircon grains to coastline areas. Other minerals such as ilmenite ($FeTiO_3$) and rutile (TiO_2) undergo this same process and are found within the same heavy-mineral sands as zircon (ZIA 2019).

The production of zircon from heavy-mineral sands consists of three primary process stages: wet or dry mining, beneficiation (also referred to as concentration), and separation. These processes are described by ZIA (2019) and Gediga et al. (2019). Dry mining involves using equipment such as scrapers, bulldozers, and excavators to obtain heavy-mineral sands from solid inland deposits, while wet mining involves employing floating dredges to remove heavy-mineral sands from water ponds. The mined product, which contains about 10%-20% heavy-mineral content, is then concentrated. Concentration is typically performed by wet gravity separation methods that use equipment such as hydrocyclones or spirals to divide the heavy-mineral sands from other lighter and non-valuable materials, producing a heavy-mineral concentrate (HMC) with an 85%-95% heavy-mineral content. For wet mining, concentration occurs within the water source using a floating concentrator in conjunction with the floating dredge, while for dry mining, a slurry is produced from the mined heavy-mineral sands to input into the concentrator on site. After concentration, the HMC is transported to a mineral separation plant (MSP) where a combination of techniques, including screening as well as magnetic, electrostatic, and gravity separation circuits, is employed to separate zircon from other minerals in the HMC such as ilmenite and rutile.

Gediga et al. (2019) provide a comprehensive life cycle inventory for zircon production from mineral sands that covers more than 77% of global zircon production. Industry data for zircon production was collected from ten different production sites from eight companies across all major heavy-mineral sand-producing countries, including Australia, South Africa, Senegal, Kenya, and the United States. Both wet and dry mining methods were included in this survey. Unit process inputs and outputs for mining and beneficiation at each site's mining facilities and for separation at each site's MSP were obtained, and Gediga et al. (2019) report the material and energy inputs and outputs for these processes as a weighted average based on each site's contribution to the total production mass.

The final sand product consists of 37% zircon, 48% ilmenite, and 15% rutile. From this data, we calculated the total material and energy inputs for the mining, beneficiation, and separation of heavy-mineral sands, and we used mass allocation to determine the material and energy inputs per ton of zircon product. These inputs are shown in Table 6. As stated in the previous section, upstream information for all material and energy inputs are found in GREET (GREET 2020), with gasoline blendstock serving as a surrogate for lubricating oil, and Al_2O_3 and H_2SO_4 acting as stoichiometrically equivalent inputs in place of $Al_2(SO_4)_3$.

Table 6. Material and energy inputs for the production of zircon

Material	**Amount per ton zircon**	
H_2SO_4	0.00276 tons	
Al_2O_3	0.00005 tons	
NaOH	0.00010 tons	
Lubricating oil	0.00110 tons	
Water	5,981 gal	
Energy	**mmBtu/ton zircon**	**Share %**
Electricity	0.728	47%
Natural gas	0.289	18%
Diesel	0.536	35%
Total energy input	1.552	

The production of zircon by mining, beneficiation, and separation of heavy-mineral sands is much less energy-intensive than palladium production by PGM mining and is comparable to niobium production by pyrochlore mining. The large water consumption can be attributed to the wet concentration process in which the heavy-mineral sands are separated from lighter material in water using hydrocyclones and spirals.

2.2.2 Production of ZrO_2 catalyst by caustic fusion and calcination

Commercial ZrO_2 can be obtained from zircon by a variety of chemical, thermal, or mechanical decomposition methods (ZIA 2019). We focused on the decomposition of zircon by caustic fusion with sodium hydroxide, as this is the most commonly used zircon decomposition method (Nielsen and Wilfing 2012) and the process for which the most detailed data could be obtained. Caustic fusion entails reacting zircon ($ZrSiO_4$) with a slight excess of NaOH at 650°C to form sodium zirconate, sodium silicate, and water, as displayed in Equation 6.

$$ZrSiO_4 + 4\,NaOH \rightarrow Na_2ZrO_3 + Na_2SiO_3 + 2\,H_2O \quad (6)$$

After cooling, the products of this reaction are crushed to form a slurry. The majority of the sodium silicate is dissolved in water, while the sodium zirconate is hydrolyzed to form soluble NaOH and insoluble hydrous zirconia (Nielsen and Wilfing 2012). The hydrous zirconia can then be separated from the other products by filtration and calcined at temperatures between 800°C and 1000°C to form commercial ZrO_2 (Primas 2007).

Material and energy inputs for ZrO_2 production from zircon are presented by Primas (2007) as overall values for zircon decomposition by caustic fusion and calcination of hydrous zirconia to form commercial ZrO_2. Primas notes that the energy inputs reported for these processes are approximations based on very similar caustic fusion and calcination processes commonly used to produce sodium silicate and aluminum oxide. Primas calculated the material inputs using stoichiometry, with an assumed 10% excess of NaOH and a 95% product yield for zircon decomposition. The intermediate hydrolysis of sodium zirconate to hydrous zirconia is assumed to require no additional material or energy inputs. Primas reports a final product composition of 50% ZrO_2 and 50% sodium silicate, so we applied mass allocation to determine the material and energy inputs per ton of commercial ZrO_2.

Because we are specifically examining the production pathway for catalyst-grade, monoclinic ZrO_2, we incorporated an additional calcination step modeled after a laboratory procedure from Shylesh et al. (2017) that produces a monoclinic ZrO_2 catalyst by calcining purchased commercial ZrO_2 at a temperature of 1073 K for 3 hours. Using the same approach explained in the previous sections and in the appendices for the laboratory production of $KNbO_3$, $NbOPO_4$, and the $Pd/NbOPO_4$ catalyst, we calculated the energy requirement for calcination by modeling thermodynamic heating of ZrO_2 in an 8,300 L Nabertherm chamber furnace (Nabertherm 2016) according to the Majeau-Bettez et al. (2011) and Dunn et al. (2015) methodology. The energy required for this calcining step is equivalent to the sum of the energy needed to heat solid ZrO_2 to the required temperature (1073 K) and the energy used to heat an 8,300 L chamber furnace to that temperature for 3 hours. Only a small additional electricity input is required for this final calcination step, and we added this value to the energy consumption for the previous stages in ZrO_2 production. In Table 7, we present the material and energy inputs for the production of 1 ton of ZrO_2 catalyst as combined totals for the caustic fusion of zircon,

calcination of hydrous zirconia, and calcination of commercial ZrO_2. All inputs apart from $ZrSiO_4$, whose production we describe, are detailed in GREET (GREET 2020).

Table 7. Material and energy inputs for the production of ZrO_2

Material	**Amount per ton ZrO_2**	
$ZrSiO_4$	0.785 tons	
NaOH	0.720 tons	
Water	194 gal	
Energy	**mmBtu/ton ZrO_2**	**Share %**
Electricity	0.440	20%
Natural gas	0.914	41%
Coal	0.023	1%
Residual oil	0.860	38%
Total energy input	2.237	

3. RESULTS AND DISCUSSION

3.1 SUMMARY OF LCA RESULTS

We used Argonne's GREET model (GREET 2020) to perform cradle-to-gate LCAs for Nb_2O_5, $KNbO_3$, $NbOPO_4$, Pd, the Pd/$NbOPO_4$ catalyst, $ZrSiO_4$, and the ZrO_2 catalyst. Fossil fuel consumption is reported in terms of energy unit (MJ) per mass unit (kg) of material produced. GHG emissions are reported in terms of mass unit (kg) of carbon dioxide equivalents (CO_2e) per mass unit (kg) of material produced. In order to report GHG emissions in terms of CO_2e, other GHGs such as CH_4 and N_2O are converted to their equivalent amounts of CO_2 using each gas's global warming potential (GWP). Water consumption is reported in terms of volume unit (gal) per mass unit (kg) of material produced. The LCA results for all new catalyst materials examined in this study are shown in Table 8**.**

Table 8. Cradle-to-gate LCA results for new catalysts and associated materials

Cradle-to-gate result	**Nb_2O_5**	**$KNbO_3$**	**$NbOPO_4$**	**Pd**	**Pd/$NbOPO_4$ catalyst**	**$ZrSiO_4$**	**ZrO_2 catalyst**
GHG emissions (kg CO_2e/kg material)	0.1	1.2	2.4	121	8.5	0.2	1.8
Fossil fuel consumption (MJ/kg material)	1.4	18.3	36.1	1,245	98.6	2.6	25.8
Water consumption (gal/kg material)	2.2	6.8	14.8	251	26.9	6.8	8.3

The cradle-to-gate GHG emissions, fossil fuel consumption, and water consumption values for Pd are significantly higher than the other catalyst materials, especially in comparison to the results for Nb_2O_5 and $ZrSiO_4$, which are also produced by mining and beneficiation methods. This can largely be attributed to the fact that the Pd content within the mixed metal PGM ore from which it is mined is less than 0.0002%, compared to an Nb_2O_5 content of 2.5% in pyrochlore ore and a $ZrSiO_4$ content of 10%-20% in heavy-mineral sands. Much more intensive processes are thus required to extract and isolate Pd from its mined ore. However, it is important to note that metals, particularly those with a high economic value like the PGMs, often display a large environmental burden during their production, but their use and end-of-life recycling typically counterbalance this impact (Santero and Hendry 2016). Catalysts that incorporate PGMs generally display higher activity than base-metal catalysts, and PGM recovery rates after recycling are very high at 98%-99% (Seymour and O'Farrelly 2012). While the system boundary of this study is cradle-to-gate, a cradle-to-grave analysis that accounts for usage and recycling would be especially beneficial in the case of Pd and the Pd/$NbOPO_4$ catalyst.

Below we provide a comparison of the LCA results for the new Pd/$NbOPO_4$ and ZrO_2 catalysts to the results for existing catalysts in the GREET model. Table 9 shows the Pd/$NbOPO_4$

and ZrO_2 catalyst results alongside results for three of the five catalysts previously implemented in GREET: Pt/γ-Al_2O_3, MoCo/γ-Al_2O_3, and ZSM-5 (GREET 2020, Wang et al. 2015).

Table 9. Comparison of new Pd/$NbOPO_4$ and ZrO_2 catalysts to existing catalysts in GREET

Cradle-to-gate result	Pd/$NbOPO_4$	ZrO_2	Pt/γ-Al_2O_3[a]	MoCo/ γ-Al_2O_3[a]	ZSM-5[a]
GHG emissions (kg CO_2e/kg material)	8.5	1.8	6.8	9.3	6.8
Fossil fuel consumption (MJ/kg material)	98.6	25.8	88.4	128.1	111.7
Water consumption (gal/kg material)	26.9	8.3	11.0	9.1	3.5

[a] Results for Pt/γ-Al_2O_3, MoCo/γ-Al_2O_3, and ZSM-5 catalysts are from the GREET model (GREET 2020).

The net GHG emissions and fossil fuel consumption for Pd/$NbOPO_4$ are very comparable to the existing catalysts in GREET, while these values for the ZrO_2 catalyst are considerably lower. On the other hand, water consumption for ZrO_2 is very similar to the existing catalysts in GREET, while the water consumption for Pd/$NbOPO_4$ is markedly higher. We explore the contributing factors to the Pd/$NbOPO_4$ and ZrO_2 LCA results in the following section.

3.2 ANALYSIS OF FACTORS CONTRIBUTING TO CATALYST BURDEN

To assist our interpretation of the LCA results for the $Pd/NbOPO_4$ and ZrO_2 catalysts, we first broke down the different materials contributing to the production of these catalysts, as shown in Figure 3**.** The major material input for the $Pd/NbOPO_4$ catalyst is the $NbOPO_4$ support, which accounts for 90% of material inputs for the catalyst. We also show the contribution of Nb_2O_5, H_3PO_4, and KOH as material precursors for the $NbOPO_4$ support; the $KNbO_3$ intermediate is accounted for by the Nb_2O_5 and KOH inputs. As the primary source of Nb, Nb_2O_5 accounts for nearly half of the material inputs for the $NbOPO_4$ support. Palladium and HNO_3 each contribute approximately 4.5% of material inputs for the catalyst, while N_2 and H_2 gas inputs are minimal. For the ZrO_2 catalyst, only two major material inputs are used: zircon and NaOH. The percentage contributions of zircon and NaOH to the total material inputs are nearly the same, with zircon contributing just over 50% and NaOH just under 50% of the material composition.

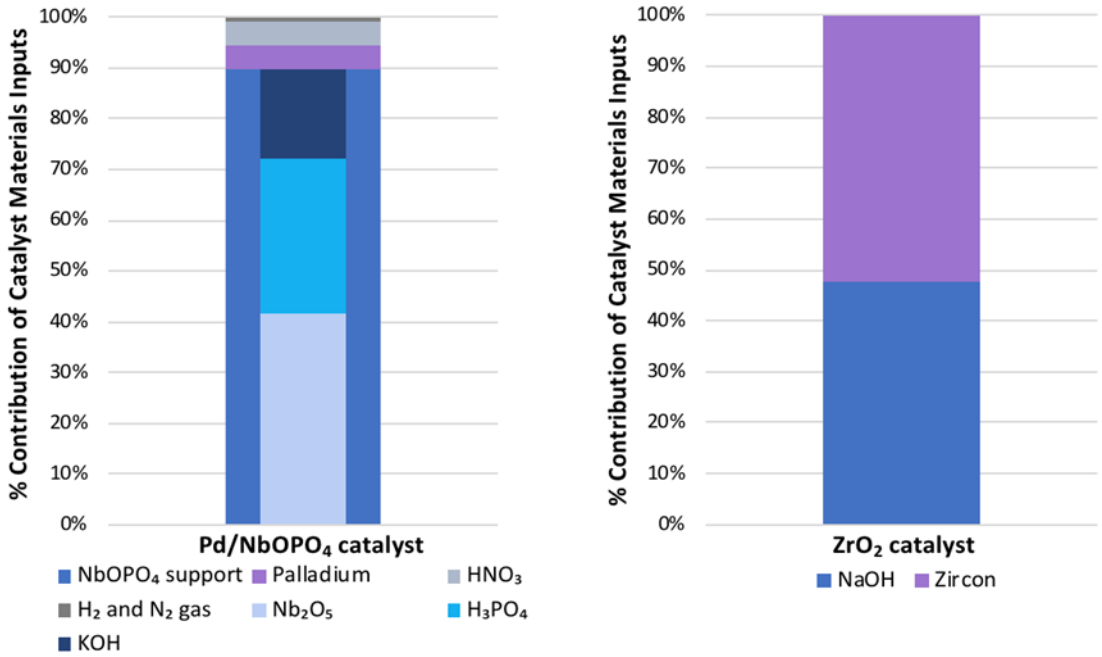

Figure 3. Contribution of material inputs to the production of a) $Pd/NbOPO_4$ and b) ZrO_2

The figures below show the contributions of the various material and energy inputs for both catalysts to the cradle-to-gate GHG emissions (Figure 4) and fossil fuel consumption (Figure 5). The proportions of each input's contribution to GHG emissions and fossil fuel consumption are very similar, which is to be expected because processes that consume large amounts of fossil fuel are also likely to exhibit large amounts of GHG emissions. Although a small amount of the energy and emissions burden is associated with additional energy inputs (electricity, natural gas, residual oil, and coal) and estimated transportation requirements for catalyst production, the majority of the environmental impact for both catalysts comes from the upstream production of their material precursors. However, for both the $Pd/NbOPO_4$ and ZrO_2

catalysts, the percent mass contribution of each material input as shown in Figure 3 is not indicative of that material's contribution to GHG emissions and fossil fuel consumption.

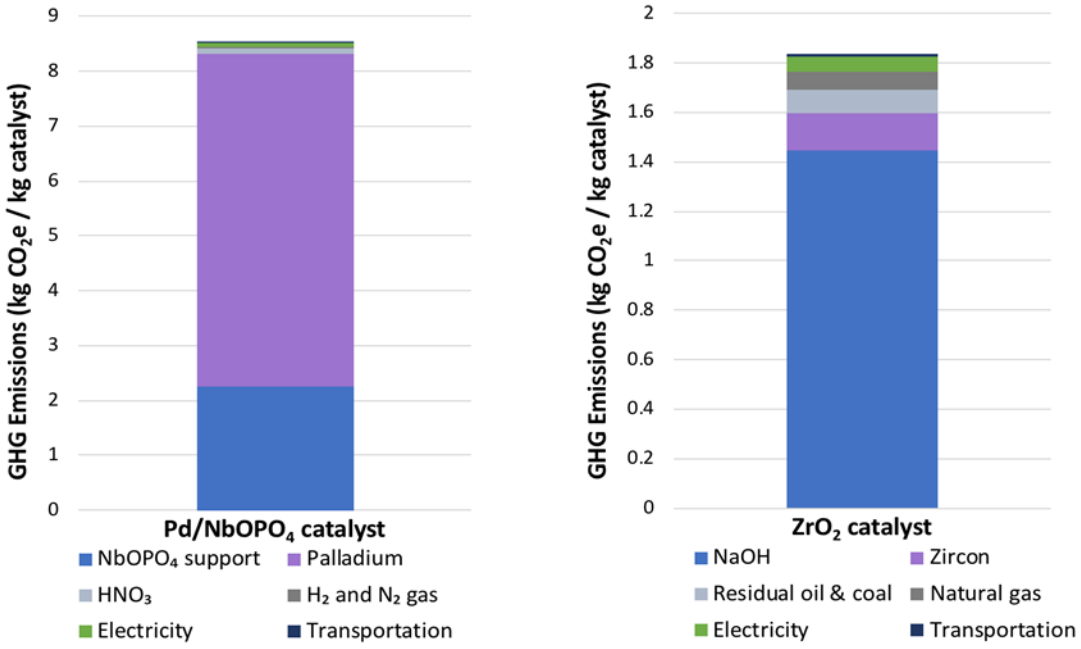

Figure 4. Breakdown of cradle-to-gate GHG emissions of a) $Pd/NbOPO_4$ and b) ZrO_2

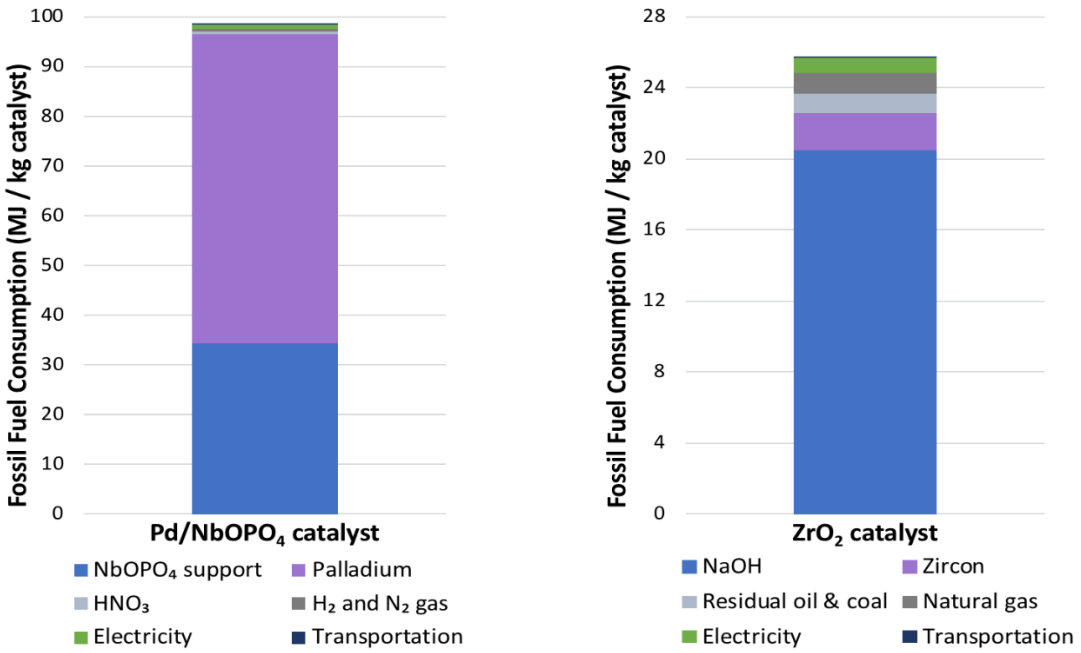

Figure 5. Breakdown of cradle-to-gate fossil fuel consumption of a) $Pd/NbOPO_4$ and b) ZrO_2

Although the primary material component of the $Pd/NbOPO_4$ catalyst by mass is the $NbOPO_4$ support, the Pd metal is by far the major contributor to cradle-to-gate GHG emissions and fossil fuel consumption—despite accounting for less than 5% of the catalyst's material inputs. This is because Pd is far more carbon-intensive than any of the other materials that are used, and its own cradle-to-gate GHG emissions and fossil fuel consumption are much higher than any other material that contributes to the $Pd/NbOPO_4$ catalyst, as we observed in Table 8**.** It is notable that the primary source of purchased energy for the production of Pd by PGM mining is electricity, contributing to 71% of the total energy consumption of Pd production, as shown in Table 4. In South Africa, 88% of electricity is sourced from coal (Kingsbury and Benavides 2021) which is also a major source of GHG emissions, leading to a high fossil fuel and emissions impact for Pd.

For the ZrO_2 catalyst, the NaOH material input is the primary contributor to cradle-to-gate GHG emissions and fossil fuel consumption despite contributing less mass than zircon to the total material inputs in catalyst production. As discussed in Section 3.1, the zircon content in the heavy-mineral sands from which it is produced is very high, so its production is minimally resource-intensive in comparison to other mining and beneficiation processes. Material and energy flows for NaOH are already detailed in GREET, so we do not describe those inputs in this study, but we note that the cradle-to-gate fossil fuel consumption of NaOH as reported in GREET (28.5 MJ/kg NaOH) is much higher than that of zircon (2.6 MJ/kg zircon), and that 73% of the fossil fuel consumption for NaOH production is from natural gas (GREET 2020).

We also examine the contributions of the various material and energy inputs of both $Pd/NbOPO_4$ and ZrO_2 to the cradle-to-gate water consumption in Figure 6**.** Process water consumption for the synthesis of both catalysts is very minimal, as is water consumed by transportation and upstream water consumption from energy inputs. The majority of water consumption is from the upstream production of the major material inputs: Pd and $NbOPO_4$ for $Pd/NbOPO_4$, and zircon and NaOH for ZrO_2. The contributions of Pd and $NbOPO_4$ to the total water consumption of the $Pd/NbOPO_4$ catalyst are nearly equivalent, while zircon has a larger impact than NaOH on water consumption for ZrO_2.

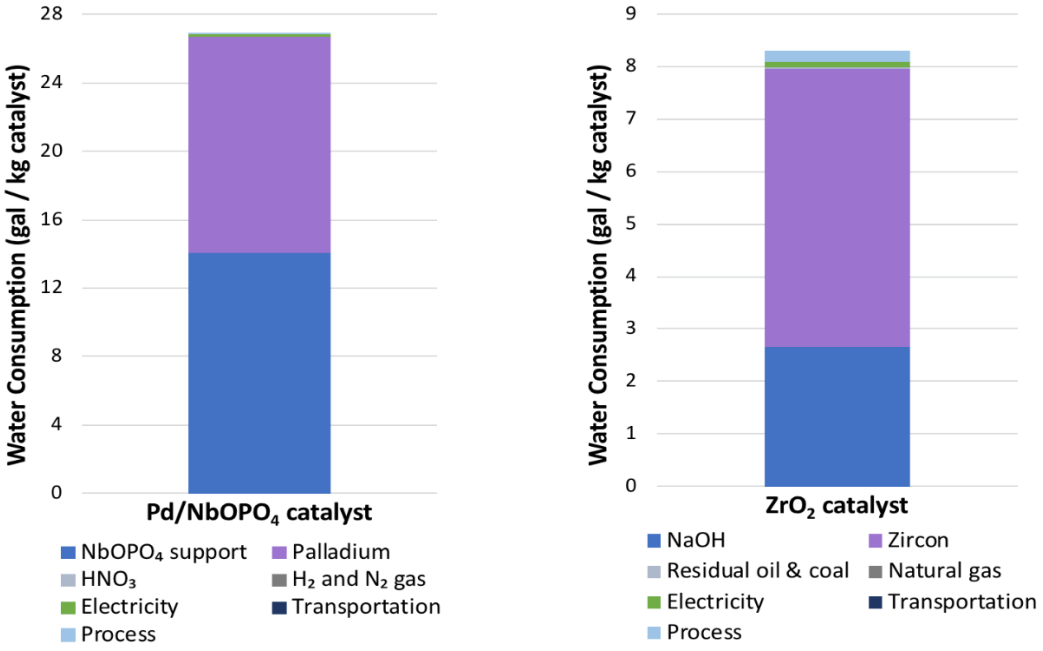

Figure 6. Breakdown of cradle-to-gate water consumption of a) $Pd/NbOPO_4$ and b) ZrO_2

The sizeable impact of zircon on the cradle-to-gate water consumption of ZrO_2 can be attributed to the wet concentration process used during heavy-mineral sands mining to increase the zircon content of the sands after mining. This explains why the ZrO_2 catalyst has a cradle-to-gate water consumption similar to other catalysts in GREET despite having lower values for cradle-to-gate GHG emissions and fossil fuel consumption. As with zircon, the concentration process for palladium production uses large amounts of water when creating a slurry to separate less valuable materials from the PGMs. A sizeable water consumption attributed to the $NbOPO_4$ support is also expected, both because the support makes up 90% of the catalyst's material inputs and because the sol–gel synthesis of $NbOPO_4$ from $KNbO_3$ and H_3PO_4 requires a large amount of water for use as a reaction solvent. The combined impact of Pd and $NbOPO_4$ causes the cradle-to-gate water consumption for this catalyst to be higher than that of the other catalysts in the GREET model. However, we note that the water consumed during production of the $NbOPO_4$ catalyst support and its $KNbO_3$ precursor is estimated based on stoichiometric assumptions from laboratory processes, which unlike industrial processes are not designed to minimize water consumption or to incorporate water recirculation. The cradle-to-gate water consumption of the $Pd/NbOPO_4$ catalyst is thus an overestimation, and there is potential to reduce water consumption if these processes were industrially optimized or if water recirculation was considered.

4. CONCLUSION

In this study, the supply chains of a $Pd/NbOPO_4$ catalyst and a ZrO_2 catalyst were identified, and LCI data was collected for each stage in the catalysts' supply chains. Material and energy flows for many materials used in the production of the $Pd/NbOPO_4$ and ZrO_2 catalysts are already detailed in GREET, while other materials such as Nb_2O_5, $KNbO_3$, $NbOPO_4$, Pd, and $ZrSiO_4$ required the compilation of new LCI data and analysis. To procure material and energy inputs for these previously undefined materials, we consulted a combination of scientific literature, technical reports, sustainability reports from mining and chemical industries, and direct correspondence with professionals in the field. Material and energy flows for the new catalysts and associated materials were implemented in GREET, and cradle-to-gate LCAs were performed. We reported cradle-to-gate values for GHG emissions, fossil fuel consumption, and water consumption for the new materials, and we examined the various factors that contribute to the environmental burden of the $Pd/NbOPO_4$ and ZrO_2 catalysts.

The cradle-to-gate GHG emissions and fossil fuel consumption of the $Pd/NbOPO_4$ catalyst are very similar to results for existing catalysts in GREET, such as $Pt/\gamma\text{-}Al_2O_3$, $MoCo/\gamma\text{-}Al_2O_3$, and ZSM-5. The primary contributing factor to emissions and fossil fuel consumption for $Pd/NbOPO_4$ is the mining and processing of the PGMs to produce Pd. The initial Pd content in PGM ore is extremely low, at less than 0.0002%, so very intensive processes of open cut mining, wet concentration, high-temperature smelting, and both physical and chemical refining are required. In addition, the main energy input for PGM production is electricity, which is almost entirely sourced from coal in South Africa, where PGMs are produced. However, the large environmental burden of Pd does not necessarily indicate that alternative metals need to be considered. PGMs have valuable catalytic properties, and their high recyclability rate (98%-99%) should be considered when putting their environmental burden in context. Although data for the secondary production of Pd was not available at this time, it would be very beneficial to incorporate recycling as a pathway for Pd production in the catalyst's LCA. There are likely to be more opportunities for reducing GHG emissions and fossil fuel consumption of $Pd/NbOPO_4$ by targeting the various processes used to synthesize the $NbOPO_4$ support, particularly those derived from laboratory procedures that are not optimized for industrial performance.

Cradle-to-gate GHG emissions and fossil fuel consumption for the ZrO_2 catalyst are smaller than those of the $Pd/NbOPO_4$ catalyst and other catalysts in GREET. This can be attributed to the facts that the ZrO_2 catalyst supply chain requires fewer production steps and that the mining and beneficiation processes for zircon are minimally intensive due to the very high initial zircon content (10%-20%) in heavy-mineral sands. It is the upstream production of NaOH, not zircon, that is the primary driver of the energy and emissions burden of ZrO_2. The environmental burden of NaOH production is mainly due to the heavy use of natural gas. While the cradle-to-gate GHG emissions and fossil fuel consumption results for the ZrO_2 catalyst are already low when compared to the other catalysts, a reduction in NaOH consumption during ZrO_2 production could be an effective option for minimizing the environmental burden of this catalyst. However, this may be difficult to achieve as excess NaOH is required for the caustic

fusion of zircon. It could be beneficial to examine potential recycling of NaOH in order to address this issue.

Both catalysts require water-intensive processes during their production. The cradle-to-gate water consumption of the $Pd/NbOPO_4$ catalyst is higher than that of the other catalysts in GREET that have comparable emissions and energy consumption results. Since one of the catalysts that we used for comparison is $Pt/\gamma\text{-}Al_2O_3$, which sources platinum (Pt) from the same PGM mining process as Pd, we can attribute the higher water consumption of the $Pd/NbOPO_4$ catalyst to the contribution of the $NbOPO_4$ support. Data on industrial-scale production of $NbOPO_4$ was unavailable, so we consulted several laboratory-scale synthetic procedures when building this inventory. Many of the chemical reactions from these laboratory procedures are conducted in water or water-based solvents, and we utilized the volume of water that the authors of these procedures report as necessary for the synthesis of a given mass of product. However, these processes are not optimized to minimize water consumption as industrial processes would be. The water consumption of $NbOPO_4$ is thus an overestimate, and it would be beneficial to examine whether the reactions involved in its production can be performed using less water. For the ZrO_2 catalyst, the main contributor to water consumption is zircon, the production of which utilizes wet gravity separation methods to separate heavy-mineral sands from less valuable mining products. Although less impactful than zircon, NaOH also contributes to the water consumption of ZrO_2, so reduction of NaOH could also help reduce water consumption.

The results of this study may be used to inform the selection of materials for the design of other catalysts or to make targeted adjustments to various stages of $Pd/NbOPO_4$ and ZrO_2 production in order to minimize environmental impacts. The system boundary of this study is cradle-to-gate, so there are more conclusions to be drawn about the ultimate environmental burden of the catalysts by accounting for end-of-life recycling and performing a cradle-to-grave analysis. In addition, the environmental burden of $Pd/NbOPO_4$ and ZrO_2 may be properly contextualized by incorporating these catalysts into LCAs of the related biofuels. Both $Pd/NbOPO_4$ and ZrO_2 have been successfully used in the production of the ether diesel bioblendstock 4-BH, so an LCA of this biofuel that includes these catalysts would be beneficial. ZrO_2 and niobic acid, a hydrated form of Nb_2O_5, have also been used in the production of diesel and jet fuel range blendstocks that merit LCAs. Due to the heavy environmental burden of producing metals, catalyst production is typically intensive, but oftentimes only a very small amount of catalyst is required for the production of a large amount of biofuel. By including catalysts in a biofuel's LCA, we can evaluate the catalyst's environmental impact in the proper context as well as obtain more accurate estimations of the life-cycle energy consumption and GHG emissions of the biofuel.

APPENDIX A: Calculation of Energy Consumption in $KNbO_3$ Production

The total energy input for the production of $KNbO_3$ is described by Equation 2. It includes three terms that require prior determination: $q_{solvent,}$ q_{CSTR}, and q_{stir}. The value of $q_{solvent}$ corresponds to the heat required to raise the temperature of the solvent to the desired reaction conditions. In this particular reaction, an 8 M KOH aqueous solution is heated from room temperature (25°C) to 200°C. We assume ideal thermodynamic heating of the KOH solution and use Equation A-1 to calculate $q_{solvent}$.

$$q_{solvent} = mC_p\Delta T \tag{A-1}$$

where:
m is the mass of solution used to produce 1 ton of $KNbO_3$ (25,174 kg);
C_p is the average specific heat capacity of an 8 M KOH solution (3387 J/kg K); and
ΔT is the change in temperature (175 K).

The value of q_{CSTR} corresponds to the heat loss of the CSTR, and it is calculated using Equation A-2 according to the methodology of Majeau-Bettez et al. (2011). The parameters λ, A, T_0, and x are specific to the reactor and are provided by Majeau-Bettez et al. (2011), while t_r and T_r are specific to the reaction and are sourced from the synthesis procedure of Lu et al. (1998).

$$q_{CSTR} = \frac{\lambda\, A\, (T_r - T_0)t_r}{x} \tag{A-2}$$

where:
λ is thermal conductivity specific to the reactor (0.04 W/mK);
A is the surface area of the reactor (25 m^2);
t_r is the reaction time (2 hours);
T_r is the temperature of the reactor (200°C);
T_0 is the temperature of the reactor wall (50°C); and
x is the thickness of the reactor insulation (0.1 m).

In this scenario, the reactants are stirred in the CSTR, so the value of q_{stir} depends on how much electricity the specific CSTR uses to agitate the reactants. Majeau-Bettez et al. (2011) report an electricity consumption of 20.92 MJ/hr for stirring the contents of the 10,000 L reactor, which must be stirred for 2 hours.

APPENDIX B: Calculation of Energy Consumption in $NbOPO_4$ Production

The total energy input for the production of $NbOPO_4$ is described by Equation 4 above. It includes seven terms: $q_{solvent}$, q_{CSTR}, q_{dry}, $q_{calcine}$, q_{oven}, $q_{furnace}$, and q_{stir}. Using the same approach as for the production of $KNbO_3$ in Appendix A, the value of $q_{solvent}$ is again calculated using Equation A-1. In the case of $NbOPO_4$ production, a 0.4 M H_3OPO_4 solution is heated incrementally from room temperature (approximately 25°C) to 40°C, to 80°C, and ultimately to 160°C. The input values for m, C_p, *and* ΔT in Equation A-1 are adjusted to correspond to the mass of H_3PO_4 solution used to produce 1 ton of $NbOPO_4$ (55,568 kg), the average specific heat capacity of a 0.4 M H_3PO_4 solution (4148 J/kg K), and the total change in temperature (135 K), respectively. The value of q_{CSTR} is calculated using Equation A-2, with the reaction-specific values for t_r and T_r being adjusted to the total heating time for $NbOPO_4$ production (27 hours) and the temperature of the reactor (160°C), respectively.

The values of q_{dry} and $q_{calcine}$ are determined in the same manner as $q_{solvent}$, using Equation A-1, assuming ideal thermodynamic heating of solid $NbOPO_4$ from room temperature to the desired final temperature for either drying (110°C) or calcining (400°C). The specific heat capacity of $NbOPO_4$ is estimated as 418 J/kg K according to the Neumann-Kopp rule, which states that the specific heat capacity of a compound may be approximated as a weighted sum of the heat capacities of its elemental constituents (Atkins and Escudier, 2019). Both q_{dry} and $q_{calcine}$ are calculated for the heating of 1 ton, or 907.185 kg, of solid $NbOPO_4$ product.

The energy used to heat the oven to 110°C for the drying step (q_{oven}) is calculated using Equation B-1 according to the methodology of Majeau-Bettez et al. (2011) and Dunn et al. (2015). The value for the heating duration *t* is provided by the synthesis procedure of He et al. (2020), while the value for power consumption *P* is estimated using data for a Nabertherm chamber oven (Nabertherm 2016). Majeau-Bettez et al. (2011) assume in their calculations that an oven does not require the electricity needed to reach its maximum heating power if it is not being heated to its maximum temperature.

We therefore apply an estimation method described by Tschernitz (2001) in which the operating power of the oven is approximated by the ratio of the operating temperature to the maximum temperature taken to the third power and multiplied by the maximum power consumption of the oven. The volume of the oven is 1,000 L, which we use to scale q_{oven} to the electricity that the oven requires for the drying of 1 ton of $NbOPO_4$.

$$q_{oven} = P \times t \tag{B-1}$$

where:
P is the operating power of the oven at 110°C (0.68 kW); and
t is the duration of heating in the oven (12 hours).

The value for $q_{furnace}$ is calculated using the same method as q_{oven} in Equation B-1, with *P* being adjusted to the operating power of a Nabertherm chamber furnace at 400°C (12.5 kW) and *t* being adjusted to the duration of heating in the furnace during the calcining step (3 hours). The volume of the furnace, 8,300 L, is used to scale the electricity consumption to 1 ton of $NbOPO_4$. Finally, q_{stir} is again determined based on an electricity consumption of 20.92 MJ/hr for stirring the contents of the 10,000 L continuous-stir tank reactor (Majeau-Bettez et al. 2011) for 3 hours.

APPENDIX C: Calculation of Energy Consumption in Pd/$NbOPO_4$ Production

The total energy input for the production of Pd/$NbOPO_4$ is described by Equation 5. It includes seven terms: q_{dry_1}, q_{dry_2}, q_{reduce}, q_{oven_1}, q_{oven_2}, q_{tube}, and q_{stir}. The values for q_{dry_1}, q_{dry_2}, and q_{reduce} are all calculated using Equation A-1 assuming ideal thermodynamic heating of solid Pd/$NbOPO_4$. For all three calculations, the input for mass m is 1 ton, or 907.185 kg, and the input for the average specific heat C_p of Pd/$NbOPO_4$ is 409 J/kg K. The change in temperature ΔT is 82 K, 240 K, and 240 K for the first drying step, the second drying step, and the reducing step, respectively.

The values of q_{oven_1}, q_{oven_2}, and q_{tube} are all calculated with Equation B-1 using the same method of estimating power consumption based on the operating temperature. We use a Nabertherm oven with a volume of 1,050 L to model drying steps at 110°C and 265°C (Nabertherm 2017). The first drying step has an operating power consumption P of 0.21 kW and a duration t of 6 hours. The second drying step has an operating power consumption P of 3.2 kW and a duration t of 2 hours. We use a Nabertherm tube furnace with a loading volume of 0.8 L to model the reduction of Pd/$NbOPO_4$ at 265°C (Nabertherm 2017). Reduction in the tube furnace requires an operating power consumption P of 0.065 kW and a duration t of 5 hours. The volumes of the oven and tube furnace are used to scale the results to the production of 1 ton of Pd/$NbOPO_4$.

The reactants used to form Pd/$NbOPO_4$ are not stirred in an autoclave or CSTR, as they are in the production of $KNbO_3$ and $NbOPO_4$, so we model the agitation of the reactants using a chemical mixer that can agitate catalyst slurries up to 1,892L (Madden Pump 2020). The mixer operates at 0.33 horsepower when stirring its maximum volume of contents, and the duration of stirring is 12 hours. Again, the energy consumption is scaled to the volume of reactants that must be stirred to produce 1 ton of Pd/$NbOPO_4$.

APPENDIX D: Inputs and Results using Market Allocation for Pd Production

In Table D-1, we provide inputs for palladium production that were calculated by Kingsbury and Benavides (2021) using a market allocation approach. These inputs serve as an alternative to the values in Table 4 that were calculated using mass allocation, which is the default allocation method in GREET (GREET 2020). The total energy input of Pd production by market allocation is more than two orders of magnitude greater than the energy input by mass allocation. This is primarily due to the high market price of Pd, which is second only to Pt when compared to the market prices of the other outputs of PGM production. Specific values for the variables used in the market allocation calculation, including the market prices and production masses of the PGMs, can be found in the report by Kingsbury and Benavides (2021).

Table D-1. Market allocation material and energy inputs for the production of palladium

Material	**Amount per ton Pd**	
Water	171,176 gal	
Energy	**mmBtu/ton Pd**	**Share %**
Electricity	90,370	71%
Diesel	14,571	11%
Coal	21,292	17%
Natural gas	1,292	1%
Total energy input	127,525	

In Table D-2, we provide the results of the cradle-to-gate LCA for both Pd and the $Pd/NbOPO_4$ catalyst using the market allocation inputs for Pd production from Table D-1.

Table D-2. Cradle-to-gate LCA results for Pd and $Pd/NbOPO_4$ using market allocation inputs

Cradle-to-gate result	**Pd**	**$Pd/NbOPO_4$ catalyst**
GHG emissions (kg CO_2e/kg material)	32,223	1,614
Fossil fuel consumption (MJ/kg material)	330,918	16,582
Water consumption (gal/kg material)	16,786	854

When compared to the cradle-to-gate LCA results for Pd and $Pd/NbOPO_4$ shown in Table 8 that used the mass allocation inputs for Pd production, the results shown in Table D-2 are significantly higher for both Pd and $Pd/NbOPO_4$. Notably, the cradle-to-gate GHG emissions and fossil fuel consumption for the $Pd/NbOPO_4$ catalyst are both more than two orders of magnitude

larger when using the market allocation inputs compared to the mass allocation inputs, and the cradle-to-gate water consumption is more than one order of magnitude larger. This causes Pd to have a much larger percent contribution to the cradle-to-gate GHG emissions, fossil fuel consumption, and water consumption of the $Pd/NbOPO_4$ catalyst since the environmental burden of Pd increases while the other components of the catalyst remain the same. When using the mass allocation inputs for Pd production, Pd accounts for 71% of the GHG emissions, 63% of the fossil fuel consumption, and 47% of the water consumption of the $Pd/NbOPO_4$ catalyst. When using the market allocation inputs, Pd accounts for over 99% of the GHG emissions and fossil fuel consumption of the $Pd/NbOPO_4$ catalyst and for over 98% of the catalyst's water consumption. Although Pd makes up only a small amount of the $Pd/NbOPO_4$ catalyst by mass, the choice of allocation method for Pd production has a significant effect on the catalyst's LCA results.

REFERENCES

- Atkins, T., and M. Escudier. 2019. *A Dictionary of Mechanical Engineering (2nd ed.).* Oxford, UK: Oxford University Press.
- Benavides, P. T., Q. Dai, J. Sullivan, J. C. Kelly, and J. B. Dunn. 2015. *Material and Energy Flows Associated with Select Metals in GREET2: Molybdenum, Platinum, Zinc, Nickel, Silicon*. https://doi.org/10.2172/1224976.
- Benavides, P. T., D. Cronauer, F. Adom, Z. Wang, and J. B. Dunn. 2017. "The influence of catalysts on biofuel life cycle analysis (LCA)." *Sustainable Materials and Technologies* 11 (1): 53-59. https://doi.org/10.1016/j.susmat.2017.01.002.
- Burnham, A., M. Wang, and Y. Wu. 2006. *Development and Applications of GREET 2.7—The Transportation Vehicle-Cycle Model*. https://doi.org/10.2172/898530.
- CatCost™ (Catalyst Cost Estimation Tool). 2019. National Renewable Energy Laboratory. https://catcost.chemcatbio.org.
- Companhia Brasileira de Metalurgia e Mineração (CBMM). 2019. *Sustainability Report.* https://cbmm.com/assets/sustainability-report-2019/en/.
- Darragh, K. V., and C. A. Ertell. 2003. "Aluminum Sulfate and Alums." In *Kirk-Othmer Encyclopedia of Chemical Technology.* Hoboken, NJ: John Wiley & Sons, Inc.
- Davis, R., N. Grundl, L. Tao, M. J. Biddy, E. C. D. Tan, G. T. Beckham, D. Humbird, D. N. Thompson, and M. S. Roni. 2018. *Process Design and Economics for the Conversion of Lignocellulosic Biomass to Hydrocarbon Fuels and Coproducts: 2018 Biochemical Design Case Update; Biochemical Deconstruction and Conversion of Biomass to Fuels and Products via Integrated Biorefinery Pathways*. https://doi.org/10.2172/1483234.
- Dunn, J. B., C. James, L. Gaines, K. Gallagher, Q. Dai, and J. C. Kelly. 2015. *Material and Energy Flows in the Production of Cathode and Anode Materials for Lithium Ion Batteries*. https://doi.org/10.2172/1224963.
- Gaspar, D. J., B. H. West, D. Ruddy, T. J. Wilke, E. Polikarpov, T. L. Alleman, A. George, et al. 2019. *Top Ten Blendstocks Derived from Biomass for Turbocharged Spark Ignition Engines: Bio-blendstocks with Potential for Highest Engine Efficiency*. https://doi.org/10.2172/1567705.
- GREET (Greenhouse gases, Regulated Emissions, and Energy use in Technology) Model. 2020. Argonne National Laboratory. https://greet.es.anl.gov/.
- Hafenstine, G., N. A. Huq, D. R. Conklin, M. R. Wiatrowski, X. Huo, Q. Guo, K. Unocic, and D. Vardon. 2020. "Single-phase catalysis for reductive etherification of diesel bioblendstocks." *Green Chem.* 22 (14): 4463-4472. https://doi.org/10.1039/D0GC00939C.
- He, M., J. Guo, X. Wang, Y. Song, S. Liu, H. Wang, and C. Li. 2020. "Direct conversion of cellulose into isosorbide over Ni doped $NbOPO_4$ catalysts in water." *New J. Chem.* 44 (25): 10292-10299. https://doi.org/10.1039/D0NJ01403F.

- Huq, N.A., X. Huo, G. R. Hafenstine, S. M. Tifft, J. Stunkel, E. D. Christensen, G. M. Fioroni, et al. 2019. "Performance-advantaged ether diesel bioblendstock production by a priori design." *Proc. Natl. Acad. Sci. U.S.A.* 116 (52): 26421-26430. https://doi.org/10.1073/pnas.1911107116.
- Kettler, P. 2003. "Platinum Group Metals in Catalysis: Fabrication of Catalysts and Catalyst Precursors." *Organic Process Research & Development* 7 (3): 342-354. https://doi.org/10.1021/op034017o.
- Kingsbury, K., and P. T. Benavides. 2021. "Update of Platinum Production and Addition of Platinum group metals (PGMs) to GREET® 2021." Unpublished.
- Lu, C.-H., S.-Y. Lo, and H.-C. Lin. 1998. "Hydrothermal synthesis of nonlinear optical potassium niobate ceramic powder." *Materials Letters* 34 (3-6): 172-176. https://doi.org/10.1016/S0167-577X(97)00170-5.
- Madden Pump. 2020. "Chemical Mixers." Accessed December 1, 2020. https://maddenpump.com/product/industrial-mixers/.
- Majeau-Bettez, G., T. R. Hawkins, and A. H. Strømman. 2011. "Life Cycle Environmental Assessment of Lithium-Ion and Nickel Metal Hydride Batteries for Plug-In Hybrid and Battery Electric Vehicles." *Environ. Sci. Technol.* 45 (10): 4548-4554. https://doi.org/10.1021/es103607c.
- Nabertherm. 2016. *Thermal Process Technology Catalog.* https://pdf.directindustry.com/pdf/nabertherm/thermal-process-technology-i/16539-459513.html.
- Nabertherm. 2017. *Thermal Process Technology II Catalog.* https://pdf.directindustry.com/pdf/nabertherm/thermal-process-technology-ii/16539-459527.html.
- Nielsen, R.H., and G. Wilfing. 2011. "Zirconium and Zirconium Compounds." In *Ullmann's Encyclopedia of Industrial Chemistry, 40th Ed.* Weinheim, Ger.: Wiley-VCH.
- Nowak, I., and M. Ziolek. 1999. "Niobium Compounds: Preparation, Characterization, and Application in Heterogeneous Catalysis." *Chem. Rev.* 99 (12): 3603-3624. https://doi.org/10.1021/cr9800208.
- Padilla, A. 2020. "Niobium (Columbium)." In *Mineral Commodity Summaries.* https://pubs.usgs.gov/periodicals/mcs2020/mcs2020-niobium.pdf.
- Primas, A. 2007. "Zirconium oxide production from mineral sands." in *Life Cycle Inventories of Chemicals Data v2.0 (2007).* https://db.ecoinvent.org/reports/08_Chemicals.pdf.
- Rashid, U., S. Soltani, S. I. Al-Resayes, and I. A. Nehdi. 2018. "Metal oxide catalysts for biofuel production." In *Metal Oxides in Energy Technologies,* edited by Y. Wu and G. Korotcenkov, 303-319. Cambridge, MA: Elsevier.
- Santero, N., and J. Hendry. 2016. "Harmonization of LCA methodologies for the metal and mining industry." *Int. J. Life Cycle Assess.* 21 (11): 1543-1553. https://doi.org/10.1007/s11367-015-1022-4.

- Schulz, K. J., N. M. Piatak, and J. F. Papp. 2017. "Niobium and Tantalum." In *Critical Mineral Resources of the United States—Economic and Environmental Geology and Prospects for Future Supply*, edited by K. J. Schulz, J. H. DeYoung, Jr., R. R. Seal II, and D. C. Bradley. Reston, VA: U.S. Geological Survey.
- Seymour, R.J., and J. O'Farrelly. 2012. "Platinum group metals." In Kirk-Othmer Encyclopedia of Chemical Technology. Hoboken, NJ: John Wiley & Sons, Inc.
- Shylesh, S., A. A. Gokhale, K. Sun, A. M Grippo, D. Jadhav, A. Yeh, C. R. Ho, and A. T. Bell. 2017. "Integrated catalytic sequences for catalytic upgrading of bio-derived carboxylic acids to fuels, lubricants and chemical feedstocks." *Sustainable Energy & Fuels* 1 (8):1805-1809. https://doi.org/10.1039/C7SE00359E.
- Sullivan, M. 2005. "Oil, Lubricating." In *Encyclopedia of Toxicology (2nd edition),* 295-297. Cambridge, MA: Academic Press.
- Tschernitz, J. 2001. "Energy in Kiln Drying." In *Dry Kiln Operator's Manual,* edited by W. Simpson, 239-256. Madison, WI: U.S. Department of Agriculture.
- Wang, X., Y. Song, C. Huang, and B. Wang. 2018. "Crystalline niobium phosphates with water-tolerant and adjustable Lewis acid sites for the production of lactic acid from triose sugars." *Sustainable Energy & Fuels* 2 (7):1530-1541. https://doi.org/10.1039/C8SE00140E.
- Wang, Z., P. T. Benavides, J. B. Dunn, and D. C. Cronauer. 2015. *Development of GREET Catalyst Module*. https://doi.org/10.2172/1224972.
- Zircon Industry Association (ZIA). 2019. *Technical handbook on zirconium and zirconium compounds*. https://www.zircon-association.org/download-handbook.html.